BIREFRINGENCE MEASUREMENTS OF STRUCTURAL INHOMOGENEITIES IN *RANA PIPIENS* ROD OUTER SEGMENTS

MICHAEL W. KAPLAN AND MARK E. DEFFEBACH, *Neurological Sciences Institute, Good Samaritan Hospital and Medical Center, Portland, Oregon 97210 and*
PAUL A. LIEBMAN, *Department of Anatomy, University of Pennsylvania School of Medicine, Philadelphia, Pennsylvania 19174 U.S.A.*

ABSTRACT The birefringence (Δn) of *Rana pipiens* rod outer segments (ROS) reveals microstructure inhomogeneities not seen with other techniques. In the basal 20–30-μm length of the ROS there is a nearly linear axial gradient in Δn of $\cong -2 \times 10^{-5}/\mu$m. No consistent Δn gradients are found in the distal 20–30 μm of the ROS. Using glycerol imbibition to separate the intrinsic and form birefringence components, we found that the basal Δn gradient was principally due to a gradient of the intrinsic birefringence component. The disk membrane volume fraction decreases uniformly from the basal end to the distal end, while the disk membrane refractive index increases. The contributions of these changes to the form birefringence approximately cancel, so that the form component is fairly uniform along the ROS axis. Because its axial distance from the inner segment is a measure of the time since a disk membrane was formed, these gradients may reflect a disk membrane aging process. Occasionally a highly birefringent, 2-μm-wide band is seen at the basal end of the ROS, possibly where the envelope membrane folds to form new disk membranes.

INTRODUCTION

Rod outer segments (ROS) are uniaxially birefringent with the optic axis parallel to the rod axis; i.e. the refractive index for light linearly polarized in planes parallel to the ROS axis, $n_\parallel$, is slightly larger than the refractive index for light polarized in planes normal to the ROS axis, $n_\perp$ (Schmidt, 1935, 1938; Weale, 1970, 1971). The birefringence, $\Delta n = n_\parallel - n_\perp$, exhibited by ROS is an additive composite of a positive intrinsic birefringence and a negative form birefringence (Liebman et al., 1974; Kaplan and Liebman, 1977). The intrinsic component is due to aligned arrays of molecules having anisotropic electronic polarizabilities, such as the phospholipids in the stacked disk membranes. The form component is due to the regular layering of the disk membranes, which have a relatively high bulk dielectric constant, within the cytoplasmic matrix, which has a lower bulk dielectric constant (Wiener, 1912).

It has recently been reported that the birefringence of *Rana pipiens* ROS is not uniform along the cell axis (Liebman, 1975). The basal end usually has a higher birefringence than the distal end. In the series of experiments described here we have further characterized this birefringence gradient by quantifying its shape, and by measuring

the relative contributions of the intrinsic and form birefringence components to the net birefringence along the ROS axis. Such measurements reveal structural inhomogeneities not readily detected by other biophysical techniques.

MATERIALS AND METHODS

Adult *Rana pipiens*, $2\frac{1}{2}$–$3\frac{1}{2}$ inches long, were kept in a 12-h light/12-h dark cycle for at least 3 days. After a 2–3 h dark adaptation period, pieces of retina were isolated under dim red illumination, as described by Liebman and Entine (1968). After brief immersion in Ringer solution containing 1.3% agar by weight at a temperature of 38–40°C, a retinal slice was swabbed along the bottom of a perfusion chamber constructed from cover slips. The solution quickly gelled, leaving isolated ROS imbedded in a thin layer of agar. Bleached ROS were prepared by exposing whole retinas to white light from a 60 W incandescent lamp placed 30 cm away for 30 min. Visual pigment is fully bleached under such conditions, and bleach-induced birefringence changes are completed (Kaplan and Liebman, 1977). Glutaraldehyde-fixed ROS were prepared by immersing whole retinas in Ringer solution containing 2.5% glutaraldehyde for 5–15 min at 20°C. The fixation flask was gently stirred approximately every 30 s to insure uniform fixation of the ROS.

The birefringence of 4-μm-wide sections along the ROS axis was measured by the rotary compensator plate method of Bear and Schmitt (1936). Outer segments were aligned on the stage of a polarizing microscope (Zeiss WL Pol fitted with birefringence-free condenser and objective lenses, Carl Zeiss, Inc., New York) with the cell axis aligned 45° from the polarizer and analyzer axes. A slit was imaged such that light intensity transmitted through a 4-μm-wide section of the ROS could be compared with the intensity transmitted through the adjacent cell-free field. A calibrated $\lambda/20$ rotary mica compensator plate positioned between the stage and the analyzer was adjusted until the intensity at the central chord of the ROS matched that of the background. Under such conditions the birefringence of the ROS section can be calculated from

$$\Delta n = -2R(\sin 2\beta)/l, \tag{1}$$

where Δn is the ROS birefringence, R is the retardation of the compensator crystal (in nanometers), β is the angle between the polarizer axis and the slow axis of the compensator, and l is the diameter (in nanometers) of the ROS. All measurements were made using light of wavelengths for which anomalous dispersion dependent birefringence effects are not a factor (Liebman et al., 1974). For dark-adapted ROS, light from a 60-W tungsten-halogen source was filtered by a deep red Wratten 70 filter. For bleached ROS, either no filter or a green Wratten 65 filter was used.

The contributions of intrinsic and form birefringence to the net birefringence were measured by the technique of glycerol imbibition (Liebman, et al., 1974; Kaplan and Liebman, 1977). We assume that the internal structure of ROS consists of multiple layers of membranes separated by cytoplasmic gel. For such a geometry the dependence of the ROS net birefringence upon the refractive indices and volume fractions of the membranes and cytoplasm is given by Eq. 2 derived from the Wiener equation for layered dielectric platelets having different bulk dielectric constants (Wiener, 1912).

$$\Delta n = \Delta n_i + \Delta n_f = \Delta n_i - [fg(m^2 - c^2)^2/2t(fc^2 + gm^2)], \tag{2}$$

where Δn is the ROS net birefringence, Δn_i the intrinsic birefringence component, Δn_f the form birefringence component, f the membrane volume fraction, g the cytoplasm volume fraction

($f + g = 1$), t the net bulk refractive index of the ROS, m the membrane bulk refractive index, and c the cytoplasm bulk refractive index.

The magnitude of the negative form birefringence component is reduced when the refractive index of the cytoplasm is increased by perfusing ROS with glycerol-containing Ringer solutions. Net birefringence is measured as a function of r, the refractive index of the imbibing glycerol solutions. A least-squares best-fit parabola is then calculated as an approximation of the Wiener equation, since Eq. 2 is a parabola to well within the experimental error of our measurements. The value of Δn at the peak of the parabola is the intrinsic birefringence of the ROS due to membrane and/or cytoplasmic constituents, since $m = c$ and the form birefringence is eliminated at that point. The value of c is related to r by,

$$c = r + d, \tag{3}$$

where d is the incremental refractive index that must be added to the refractive index of the imbibing medium to correct for solids in the cytoplasmic matrix. The value of r at the peak of the parabola, p, is related to m by

$$m = p + d. \tag{4}$$

In an earlier paper (Liebman et al., 1974) we incorrectly omitted the incremental refractive index term from this equation and thus reported values for m that were slightly lower than those reported here. The value of d is related to the cytoplasmic solids content, s, by,

$$d = 0.0018s, \tag{5}$$

when s is expressed in grams per 100 ml of solvent (Barer, 1966). Since t is a composite of the membrane and cytoplasm refractive indices, it is also a function of r. Expressed as a weighted sum of the membrane and cytoplasm dielectric constants (squared refractive indices),

$$t = [f(p + d)^2 + g(r + d)^2]^{1/2}. \tag{6}$$

Eq. 2 rewritten in terms of the experimental parameters thus becomes

$$\Delta n = \Delta n_i - \frac{f(1 - f)[(p + d)^2 - (r + d)^2]^2}{2[f(p + d)^2 + (1 - f)(r + d)^2]^{1/2}[f(r + d)^2 + (1 - f)(p + d)^2]}. \tag{7}$$

The procedure used for finding the values of f and d giving the closest fit of Eq. 7 to the parabola determined from the experimental data is as follows. Iterative calculations of Δn as a function of r are first done with various values of f and an assumed value of $d = 16$. The form birefringence term in Eq. 7 is not very sensitive to changes in d, so the cytoplasmic solids content is more reliably determined from a modified form of Eq. 6. Sidman (1957) found that $t = 1.4106$ for frog ROS using index-matching techniques. The value of f giving the best fit to the data in the initial calculations is used to calculate d from

$$1.4106 = [f(p + d)^2 + (1 - f)(1.335 + d)^2]^{1/2}, \tag{8}$$

since $r = 1.335$ for aqueous Ringer solution. The d derived from Eq. 8 is then used in a recalculation of f using Eq. 7. If the new f differs from the initially derived value, the procedure is repeated until no further changes in f or d result from the substitutions.

The glycerol imbibition technique therefore yields information about the intrinsic birefrin-

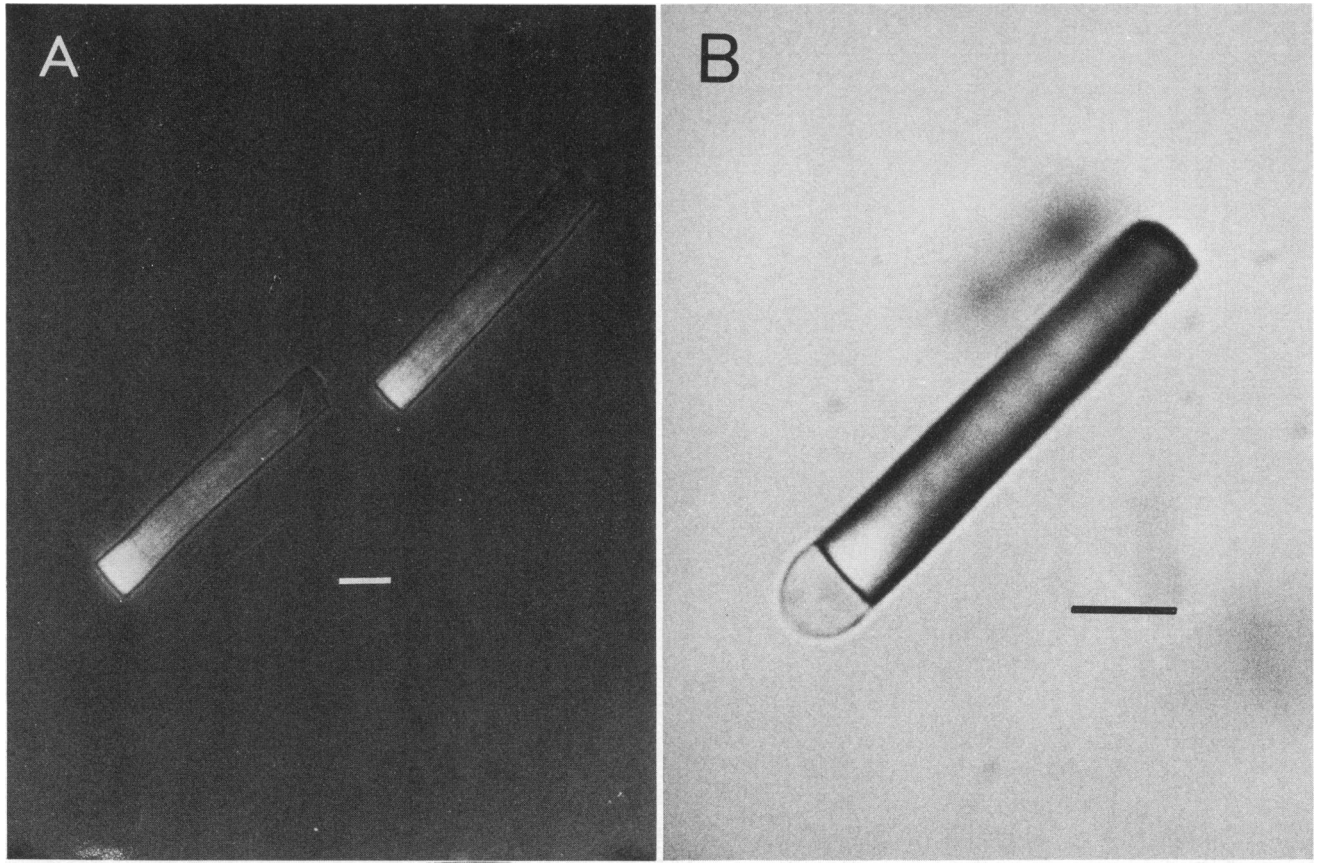

FIGURE 1 (A) Frog ROS viewed with axes aligned at a 45° angle from the polarizer and analyzer axes. Compensator plate is adjusted for intensity match of background with middle of ROS. The brighter end has a higher intrinsic birefringence. (B) Outer segment with ellipsoid attached showing that the basal end containing the youngest membranes is more birefringent. Scale bars are 10 μm long.

gence, membrane volume fraction, membrane refractive index, and cytoplasmic solids content for any point along the ROS axis.

Rhodopsin concentration and dichroism along the ROS axis were measured with a computer-controlled scanning microspectrophotometer based upon the design of Liebman and Entine (1964). The measuring beam was formed by imaging a circular aperture onto the ROS with an inverted microscope consisting of a Zeiss K 10.1 UV projective lens and a 25×/0.60n.a. Pol objective lens. At the image plane the beam had a diameter of 5 μm. The signal-to-noise ratio for the measurement allowed optical density differences of 0.002 to be resolved, or about 3% of the peak value at 502 nm. Measurements were made at the basal end, the midpoint, and the distal end of the ROS in a search for gradients of pigment concentration and/or alignment correlated with the birefringence gradients.

RESULTS

Birefringence Gradients

The typical appearance of *Rana pipiens* ROS when viewed between crossed polarizers is shown by the examples in Fig. 1. Birefringence is highest at the basal end of the ROS, as identified by those ROS that still have attached ellipsoids (about 20% of the cells in our preparations). Birefringence gradually decreases along the ROS axis with increasing distance from the inner/outer segment junction. This birefringence gradient is seen in dark-adapted and fully bleached ROS. Its general appearance is independent of the osmotic integrity of the envelope membrane as determined by perfusing the ROS with Ringer solution containing 30% by weight impermeant sucrose. Intact ROS are permanently shrunk by such a procedure.

Occasionally a highly birefringent band ($\Delta n \simeq 0.0040$) about 2 μm wide is seen at the extreme basal end of the ROS, possibly in the region where new disk membranes

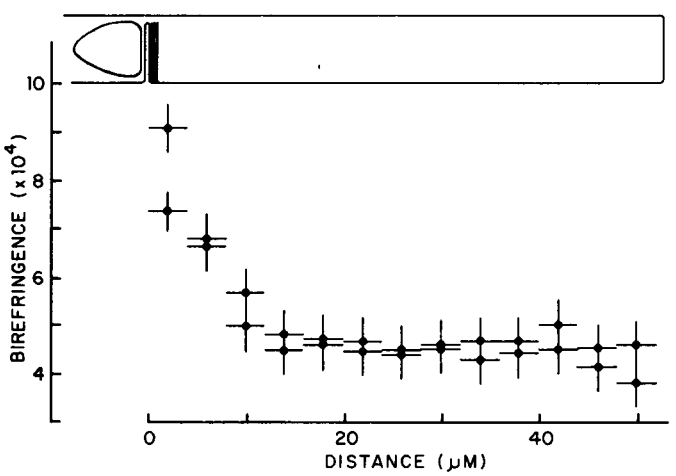

FIGURE 2 Typical birefringence pattern of frog ROS showing steep birefringence gradient in basal portion and uniform birefringence in the distal portion. Results from two scans of the same cell are shown. Vertical bars are estimates of uncertainty for a single measurement; horizontal bars show width of the measuring beam.

are forming from infolded envelope membrane. The band may reflect a specialized structuring associated with disk genesis. On the other hand, since the band was seen in fewer than 20% of the ROS studied, it may be an artifact produced in some cells when the outer segment breaks away from the inner segment. In a few cases the band was seen in isolated ROS with the ellipsoid attached, but could not be observed in ROS still attached to the retina because of light-scattering artifacts.

A quantitative plot of birefringence as a function of position along the ROS axis for a typical bleached rod is shown in Fig. 2. The birefringence gradient is not uniform. In the basal $\frac{1}{3}$ to $\frac{1}{2}$ of the ROS (15–25 μm), an approximately linear gradient of $\simeq 2 \times 10^{-5}\,\mu m^{-1}$ is usually seen (eg. Δn decreases from 0.0009 to 0.0005). Comparisons of linear versus semi-log plots of the basal gradient were inconclusive in showing that the basal gradient is either linear or logarithmic. No consistent Δn gradients are resolved in the distal $\frac{2}{3}$ to $\frac{1}{2}$ of the ROS.

Glycerol Imbibition

The contributions of intrinsic and form birefringence to the net birefringence and the Δn gradients along the ROS axis were measured with glycerol imbibition to raise the cytoplasmic refractive index. The birefringence gradient seen in normal Ringer solution is maintained as the form birefringence component is reduced.

For unfixed ROS, cell morphology and birefringence are stable for long periods when imbibed with up to 40% glycerol-Ringer solutions. At that glycerol concentration, $r = 1.385$ and about $\frac{2}{3}$ of the form birefringence is eliminated. The birefringence gradient is qualitatively the same when unfixed ROS are imbibed with 40% glycerol-Ringer solution as when they are in normal Ringer solution. Quantitative analysis is difficult with unfixed ROS because raising the glycerol content of the imbibing solution above 40% for the long periods needed to complete our measurements often caused cell deterioration, so the range of usable r values was limited. Villermet and Weale (1969) reported that ROS become distorted in Ringer solutions containing more than 15% glycerol. We see such gross morphology changes only when the ROS are exposed to abrupt incremental changes in glycerol concentration. In our experiments, the changes in glycerol concentration for sequential perfusing media was never more than 10%. Matthews et al. (1963) observed that pure glycerol denatures cattle rhodopsin solubilized in 1% digitonin, and that lower glycerol concentrations affect the metarhodopsin I $\rightleftharpoons$ metarhodopsin II equilibrium. The relevance of this observation to our experiments is uncertain, but it should be recognized that glycerol is not totally innocuous in some circumstances.

Values for f, m, s, Δn_i and Δn_f are more reliably determined in glutaraldehyde-fixed ROS than in fresh ROS, because r can be raised to 1.468 using 100% glycerol-Ringer solution without visibly damaging the cells. The minimal glutaraldehyde fixation used in our experiments reduces the net birefringence by about 0.0005 uniformly along the ROS. However, the birefringence gradient appears to be unaffected by fixing the retina in 2.5% glutaraldehyde for up to several hours. The reduction in net birefringence caused by gluteraldehyde fixation has been reported previously (Villermet and Weale, 1969; Weale, 1971), but the birefringence gradient was not resolved in the

earlier observations. Loss of net birefringence might result from changes in structural ordering and a consequent reduction of intrinsic Δn as membrane proteins and lipids containing amino groups are cross-linked to one another by glutaraldehyde polymers (Wood, 1973; Monsan et al., 1975). Alternatively, glutaraldehyde deposition might cause an increase in the membrane refractive index, thereby increasing the negative form Δn component. We found no correlation between membrane refractive index and fixation time over a range of 5–15 min.

A typical example of birefringence measured as a function of the imbibing glycerol solution's refractive index at three points along the axis of a bleached, glutaraldehyde-fixed ROS is shown in Fig. 3. Lines connecting the data points are the least squares best-fit parabolas. The ordinate values of the maxima show that the intrinsic Δn of the basal point is 0.0004 higher than the intrinsic Δn of the other two measured points at the middle and distal end of the cell. The curve for the distal point is shifted to the right of the other two curves, indicating that the membrane bulk refractive index is higher. The distal curve is also slightly flatter than the other two, indicating that the membrane volume fraction is lower than at the other two points.

The averaged results of measuring glycerol imbibition curves at the basal end, middle, and distal points of 20 frog ROS are given in Table I. The large standard deviations of the averaged values result from relatively large differences in the parameters between cells. However, when the data are analyzed as differences within a given cell, the following results are found to be significant (see Table II).

(*a*) The gradient of net Δn is principally due to a gradient in the intrinsic Δn component. (*b*) On the average, the relative volume fraction occupied by disk membranes is slightly higher at the basal end of the ROS than at the distal end. Unlike the Δn gradient, the change in volume fraction is relatively uniform along the cell. (*c*) The bulk refractive index of the disk membranes increases significantly from the basal end

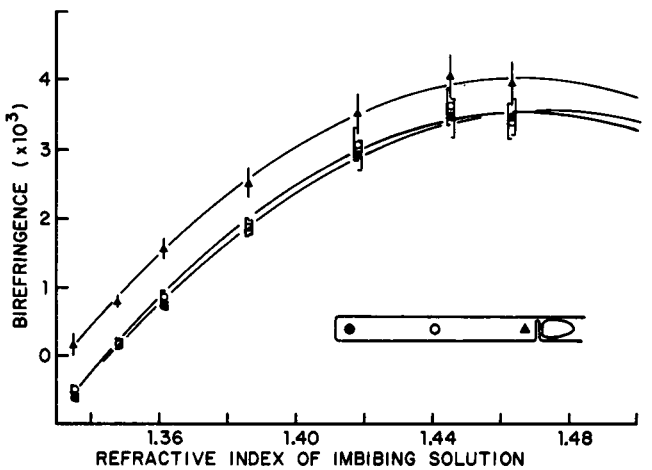

FIGURE 3 Birefringence measured as a function of imbibing glycerol-Ringer solution refractive index for three points on a glutaraldehyde-fixed frog ROS. Connecting lines are best-fit Wiener equation plots for the data.

TABLE I

AVERAGED RESULTS FROM PLOTS OF BIREFRINGENCE VS. REFRACTIVE INDEX OF IMBIBING GLYCEROL-CONTAINING RINGER SOLUTION FOR 20 BLEACHED, GLUTARALDEHYDE-FIXED FROG ROS

Distance from basal end	Basal point 0–4 μm	Midpoint 20–28 μm	Distal point 41–55 μm
Net Δn ($\times 10^4$)	3 ± 3	-4 ± 3	-4 ± 3
Intrinsic Δn ($\times 10^4$)	37 ± 7	30 ± 4	31 ± 5
Form Δn ($\times 10^4$)	-34 ± 6	-34 ± 6	-35 ± 6
Membrane volume fraction	0.28 ± 0.11	0.25 ± 0.09	0.22 ± 0.08
Membrane refractive index	1.492 ± 0.018	1.498 ± 0.014	1.508 ± 0.017
Cytoplasmic solids, *g/100 ml*	24 ± 6	25 ± 5	26 ± 4

to the distal end of the ROS. The rate of increase is noticeably greater in the distal half of the cell. (*d*) The concentration of cytoplasmic solids is uniform along the ROS. (*e*) Compensating effects of a decreasing membrane volume fraction and an increasing membrane refractive index cause the form Δn component to be approximately the same along the ROS.

Pigment Concentration and Dichroism

The optical densities for light polarized parallel to the cell axis, $A_\parallel$, and normal to the cell axis, $A_\perp$, were measured at the basal end, midpoint, and distal end in 36 ROS. Differences in optical density greater than the noise limits were usually seen for the three positions (Fig. 4). However, the points having the highest and lowest pigment concentration and/or dichroism ($A_\perp/A_\parallel$) varied from cell to cell. Therefore no pattern of differences in either the pigment concentration or dichroism were found that could be correlated with the birefringence gradients or with possible form dichroism effects (Israelachvilli et al., 1976). This result is consistent with the previous findings of Liebman (1962) and Wolken (1963).

DISCUSSION

The molecular source of the intrinsic Δn gradient seen in *Rana pipiens* ROS has not been identified. On the average, the intrinsic Δn component decreases by about 20% between the basal end and the middle of the ROS. The membrane volume fraction only decreases by about 10% over the same distance, so the steep Δn gradient in the basal portion of the cell cannot be attributed to a simple decrease in the membrane

TABLE II

AVERAGED DIFFERENCES OF PARAMETERS MEASURED WITHIN A GIVEN CELL

	Midpoint – basal point	Distal point – midpoint	Distal point – basal point
Δ(Intrinsic Δn) ($\times 10^4$)	-7 ± 3	1 ± 2	-6 ± 4
Δ(Membrane volume fraction)	-0.02 ± 0.04	-0.03 ± 0.05	-0.05 ± 0.03
Δ(Membrane refractive index)	0.006 ± 0.012	0.010 ± 0.012	0.016 ± 0.013

For other parameters, averaged differences were less than the standard deviation of the measurements.

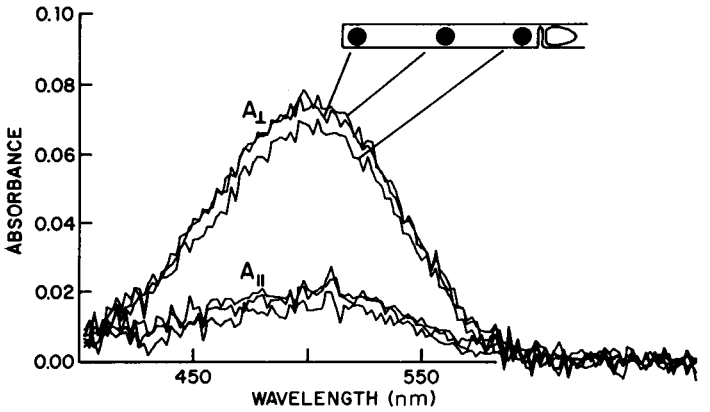

FIGURE 4 Absorbance measurements for light linearly polarized parallel ($A_\parallel$) and perpendicular ($A_\perp$) to the cell axis at three points along the outer segment. In this particular cell pigment concentration is slightly lower at the basal point than at the middle and distal points. But such differences varied from cell to cell. No patterns of optical density or dichroism ($A_\perp / A_\parallel$) differences were found that corresponded to observed birefringence gradients.

volume fraction. A portion of the change must be due to a realignment of some anisotropic constituent. Such a constituent could be in either the membrane, the intra-discal space, or the inter-discal cytoplasm. Among the many possible causes are lipid autooxidation, opsin conformation changes, concentration gradients of membrane constituents such as cholesterol or retinol, or the realignment of polysaccharides in the cytoplasmic matrix. Within the resolution limits of the techniques, microspectrophotometric measurements show that rhodopsin concentration and alignment are not correlated with the Δn gradients.

The increase in membrane bulk refractive index as the disk membrane ages could be due to an increase in the bulk refractive index of the lipid and/or protein phases, or to an increase in the relative volume fraction of protein in the membrane, or to some combination of all three processes.

Much of the increase in membrane refractive index can be accounted for by assuming that the concurrent decrease in membrane volume fraction is due to a loss of lipids only. Such an assumption is reasonable since lipid components are free to exchange in and out of ROS membranes (Bibb and Young, 1974*a*, *b*), whereas proteins are not (Young, 1967). The resulting increase in protein volume fraction would produce a higher membrane refractive index, since proteins have higher refractive indices than lipids (Israelachvilli et al., 1976). The average lipid composition of frog ROS membranes has been measured by Anderson and Risk (1974). Calculating the average lipid refractive index using their data and the measured (Weast, 1976) or calculated (Gunstone, 1958) refractive indices of fatty acids found in the membranes yields a value of $n_{lip} = 1.465$. This result is fairly close to the average refractive index of egg lecithin bilayers ($n = 1.475$) measured by Cherry and Chapman (1969). By assuming an average membrane volume composition of 0.54 protein and 0.46 lipid (Israelachvilli et al., 1976), and an average membrane refractive index of 1.499 (see Table I), the average refractive index of the membrane protein component is calculated to be $n_{prot} = 1.527$

from

$$m^2 = 0.54n_{prot}^2 + 0.46n_{lip}^2. \quad (9)$$

With $n_{prot} = 1.527$, $n_{lip} = 1.465$, and protein volume fractions calculated on the assumption that changes in f are due to a loss of lipids only, the calculated membrane refractive indices of the basal point, middle point, and distal point are $m = 1.495$, 1.499, and 1.504, respectively, if the protein volume fraction is 0.54 at the middle point. Thus approximately half of the measured change in membrane refractive index (Table I) can be accounted for by the lipid loss hypothesis.

Autooxidation of membrane lipid fatty acids could affect the membrane refractive index in several ways. Outer segment membranes have a high content of polyunsaturated fatty acids (Anderson and Risk, 1974) that are highly susceptible to oxidation. In the absence of vitamin E or other antioxidants, significant amounts of hydroperoxides form in ROS (Kagan et al. 1973; Farnsworth and Dratz, 1976) in a free-radical chain reaction that can cause scission, double bond migration, and/or *cis* to *trans* isomerization (Gunstone, 1958). It is therefore reasonable to speculate that over the 6-wk life-span of an ROS disk membrane, the content of *cis* unsaturated fatty acids is reduced. Such a reduction should produce tighter packing of lipids in the older membranes (Stryer, 1975), thereby raising the membrane refractive index. On the other hand, shorter, more saturated fatty acids have lower refractive indices than long, polyunsaturated fatty acids, so oxidative scission might reduce the membrane refractive index instead (Gunstone, 1958).

Our glycerol imbibition experiments are based upon the assumption that ROS are simple composite bodies of alternating layers of two dielectrics, and that glycerol only affects the dielectric constant of the cytoplasmic phase. Some partitioning of glycerol into the disk membranes is likely. Katz and Diamond (1974) report that dilute glycerol has a partition coefficient of 0.05 between dimyristoyl lecithin liposomes and water at 25°C. A similar partitioning between disk membrane lipids and cytoplasmic water of the relatively concentrated glycerol used in our experiments could affect the values for membrane refractive index determined by the imbibition technique. Similarly the gradient of membrane refractive index that we find might result from differential partitioning of glycerol. If so, it is still valid to conclude that disk membranes in the basal region of ROS are in some way different from those in the distal region.

Membrane volume fractions derived from X-ray diffraction and electron microscopy studies are almost twice as large as the value found in our experiments (see tabulation in Korenbrot et al., 1973). Neutron diffraction experiments using frog ROS show that the region of the interface between membrane and cytoplasm occupied by phospholipid polar headgroups is approximately one-half water by volume (Saibil et al., 1976). Presumably this volume is accessible to imbibing glycerol, so that the membrane volume fractions in Table I should be lower than those found with techniques that include the interface region as a homogeneous part of the membrane. The membrane volume fraction differences along the ROS axis reported in Table I are too small to be detected by the other techniques.

Since distance from the inner segment/outer segment junction is also a measure of

disk membrane age (Young, 1967), gradients of birefringence in ROS reflect submicroscopic organizational differences between new disk membranes and old disk membranes. Adult *Rana pipiens* maintained on a 12-h light/12-h dark cycle produce new disk membranes at a rate sufficient to add 0.84 μm/day to the basal end of their ROS (Besharse et al., 1977*a*). Studies with *Xenopus laevis* tadpoles show that more disks are formed during the first 8 h of light than at other times, so disk displacement is initially highest at that time (Besharse, et al., 1977*b*). After a few days of migration, the period of greatest disk displacement is later in the light/dark cycle, leading to the conclusion that waves of compressive stress propagate along the ROS axis and that there are local variations in disk packing density. The intrinsic birefringence gradient in the basal end of ROS could be a manifestation of such stresses in a differentially elastic system. However, without further information about the underlying mechanisms of disk propagation, such a model is purely speculative.

The interesting possibility exists that the age-dependent reordering of some disk membrane constituent plays a role in regulating membrane shedding. The process of disk shedding at the distal tips of ROS must somehow discriminate between old membranes and young membranes. It seems unlikely that the intrinsic birefringence gradient directly reflects the controlling age signal, since the underlying reduced crystallinity is nearly completed within the basal half of the ROS. However, it may reflect a change responsible for initiating a secondary process that in turn leads to an appropriate signal. Alternatively, the signal may be an altered state of the membrane's lipid phase that gives rise to an increasing membrane bulk refractive index. O'Brien (1976) has found evidence for glycosyl transferase activity in the distal portion of ROS that adds galatose and fucose molecules to the rhodopsin carbohydrate moeity. He hypothesizes that this addition may serve to signal that the disk membrane is ready to be shed and phagocytized. If, as O'Brien speculates, activation of such glycosyl transferases depends upon their lipid environment, it may be that membrane realignment and/or condensation are inducing the more active state.

This research was supported by Public Health Service grant EY01779 from the National Eye Institute, and by a grant from the Oregon Lions Sight Foundation.

Received for publication 21 November 1977.

REFERENCES

ANDERSON, R. E., and M. RISK. 1974. Lipids of ocular tissues. IX. The phospholipids of frog photoreceptor membranes. *Vision Res.* **14**:129–131.

BARER, R. 1966. Phase contrast and interference microscopy in cytology. *Phys. Tech. Biol. Res.* **3**:1–56.

BEAR, R. S., and F. O. SCHMITT. 1936. The measurement of small retardations with the polarizing microscope. *J. Opt. Soc. Am.* **26**:363–364.

BESHARSE, J. C., J. G. HOLLYFIELD, and M. E. RAYBORN. 1977*a*. Photoreceptor outer segments: accelerated membrane renewal in rods after exposure to light. *Science (Wash, D.C.).* **196**:536–538.

BESHARSE, J. C., J. G. HOLLYFIELD, and M. E. RAYBORN. 1977*b*. Turnover of rod photoreceptor outer segments. II. Membrane addition and loss in relationship to light. *J. Cell Biol.* **75**:507–527.

BIBB, C., and R. W. YOUNG. 1974*a*. Renewal of fatty acids in the membranes of visual cell outer segments. *J. Cell Biol.* **61**:327–343.

BIBB, C., and R. W. YOUNG. 1974*b*. Renewal of glycerol in the visual cells and pigment epithelium of the frog retina. *J. Cell Biol.* **62**:378–389.

CHERRY, R. J., and D. CHAPMAN. 1969. Optical properties of black lipid films. *J. Mol. Biol.* **40**:19–32.

FARNSWORTH, C. C., and E. A. DRATZ. 1976. Oxidative damage of retinal rod outer segment membranes and the role of vitamin E. *Biochim. Biophys. Acta.* **443**:556–570.

GUNSTONE, F. D. 1958. An Introduction to the Chemistry of Fats and Fatty Acids. John Wiley & Sons, Inc., New York. 77–123.

ISRAELACHVILLI, J. N., R. SAMMUT, and A. W. SNYDER. 1976. Birefringence and dichroism of photoreceptors. *Vision Res.* **16**:47–52.

KAGAN, V. E., A. A. SHVEDOVA, K. N. NOVIKOV, and Y. P. KOZLOV. 1973. Light-induced free radical oxidation of membrane lipids in photoreceptors of frog retina. *Biochim. Biophys. Acta.* **330**:76–79.

KAPLAN, M. W., and P. A. LIEBMAN. 1977. Slow bleach-induced birefringence changes in rod outer segments. *J. Physiol. (Lond.).* **265**: 657–672.

KATZ, Y., and J. M. DIAMOND. 1974. Thermodynamic constants for nonelectrolyte partition between dimyristoyl lecithin and water. *J. Membr. Biol.* **17**:389–398.

KORENBROT, J. I., D. T. BROWN, and R. A. CONE. 1973. Membrane characteristics and osmotic behavior of isolated rod outer segments. *J. Cell Biol.* **56**:389–398.

LIEBMAN, P. A. 1962. *In situ* microspectrophotometric studies on the pigments of single retinal rods. *Biophys. J.* **2**:161–178.

LIEBMAN, P. A. 1975. Birefringence, dichroism and rod outer segment structure. *In* Photoreceptor Optics, A. W. Snyder, and R. Menzel, Editors. Springer-Verlag K G., Berlin, W. Germany. 199–214.

LIEBMAN, P. A., and G. ENTINE. 1964. Sensitive low-light-level microspectrophotometer detection of photosensitive pigments of retinal cones. *J. Opt. Soc. Am.* **54**:1451–1459.

LIEBMAN, P. A., and G. ENTINE. 1968. Visual pigments of the frog and tadpole (*Rana pipiens*). *Vision Res.* **8**:761–775.

LIEBMAN, P. A., M. W. KAPLAN, W. S. JAGGER, and F. G. BARGOOT. 1974. Membrane structure changes in rod outer segments associated with rhodopsin bleaching. *Nature (Lond.).* **251**:31–36.

MATTHEWS, R. G., R. HUBBARD, P. K. BROWN, and G. WALD. 1963. Tautomeric forms of metarhodopsin. *J. Gen. Physiol.* **47**:215–240.

MONSAN, P., G. PUZO, and H. MAZARGUIL. 1975. Etude du mécanisme d'établissement des liaisons glutaraldéhyde-protéines. *Biochimie (Paris).* **57**:1281–1292.

O'BRIEN, P. 1976. Rhodopsin as a glycoprotein: a possible role for the oligosaccharide in phagocytosis. *Exp. Eye Res.* **23**:127–137.

SAIBIL, H., M. CHABRE, and D. WORCESTER. 1976. Neutron diffraction studies of retinal rod outer segment membranes. *Nature (Lond.).* **262**:266–270.

SCHMIDT, W. J. 1935. Doppelbrechung, Dichroismus und Feinbau des Aussengleides der Sehzellen vom Frosch. *Z. Zellforsch. Mikrosk. Anat.* **22**:485–522.

SCHMIDT, W. J. 1938. Polarisationoptische Analyse eines Eiwiss-Lipoid-Systems, erläutert am Aussengleid der Sehzellen. *Kolloidz.* **85**:137–148.

SIDMAN, R. L. 1957. The structure and concentration of solids in photoreceptor cells studied by refractometry and interference microscopy. *J. Biophys. Biochem. Cytol.* **3**:15–30.

STRYER, L. 1975. Biochemistry. W. H. Freeman & Company, Publishers, San Francisco, Calif. 247–249.

VILLERMET, G. M., and R. A. WEALE. 1969. The optical activity of bleached retinal receptors. *J. Physiol. (Lond.).* **201**:425–435.

WEALE, R. A. 1970. Optical properties of photoreceptors. *Br. Med. Bull.* **26**:134–137.

WEALE, R. A. 1971. On the birefringence of rods and cones. *Pflügers Arch. Ges. Physiol.* Menchen Tiere. **329**:244–257.

WEAST, R. C., editor. 1976. *Handbook of Chemistry and Physics.* CRC Press, Cleveland, Ohio. 57th edition. C75–C541.

WIENER, O. 1912. Die Theorie des Mischkörpers für das Feld der stationären Strömung. Erste Abhandlung: Die Mittlewertaätze fur Kraft, Polarisation und Energie. *Abh. Saechs. Akad. Wiss. Leipz.* **32**:507–604.

WOLKEN, J. J. 1963. Structure and molecular organization of retinal photoreceptors. *J. Opt. Soc. Am.* **53**:1–19.

WOOD, J. G. 1973. The effect of glutaraldehyde and osmium on the proteins and lipids of myelin and mitochondria. *Biochim. Biophys. Acta.* **329**:118–127.

YOUNG, R. 1967. The renewal of photoreceptor cell outer segments. *J. Cell Biol.* **33**:61–72.